International Journal of Nanomedicine

Dovepress
open access to scientific and medical research

Open Access Full Text Article

ORIGINAL RESEARCH

# In vitro and in vivo Evaluation of the Bioactive Nanofibers-Encapsulated Benzalkonium Bromide for Accelerating Wound Repair with MRSA Skin Infection

Lei Ran*, Shi-Ya Peng*, Wei Wang, Qian Wu, Yuan-Chao Li, Ru-Peng Wang

Department of Rheumatology and Dermatology, Xinqiao Hospital, Third Military Medical University of Chinese PLA, Chongqing, 430037, People's Republic of China

*These authors contributed equally to this work

Correspondence: Ru-Peng Wang, Department of Rheumatology and Dermatology, Xinqiao Hospital, Third Military Medical University of Chinese PLA, Chongqing, 430037, People's Republic of China, Email wrp71@163.com

Video abstract

Point your SmartPhone at the code above. If you have a QR code reader the video abstract will appear. Or use: https://youtu.be/wBXjQQOPzyc

**Purpose:** Developing the ideal drug or dressing is a serious challenge to controlling the occurrence of antibacterial infection during wound healing. Thus, it is important to prepare novel nanofibers for a wound dressing that can control bacterial infections. In our study, the novel self-assembled nanofibers of benzalkonium bromide with bioactive peptide materials of IKVAV and RGD were designed and fabricated.

**Methods:** Different drug concentration effects of encapsulation efficacy, swelling ratio and strength were determined. Its release profile in simulated wound fluid and its cytotoxicity were studied in vitro. Importantly, the antibacterial efficacy, inhibition of biofilm formation effect and wound healing against MRSA infections in vitro and in vivo were performed after observing the tissue toxicity in vivo.

**Results:** It was found that the optimized drug load (0.8%) was affected by the encapsulation efficacy, swelling ratio, and strength. In addition, the novel nanofibers with average diameter (222.0 nm) and stabile zeta potential (−11.2 mV) have good morphology and characteristics. It has a delayed released profile in the simulated wound fluid and good biocompatibility with L929 cells and most tissues. Importantly, the nanofibers were shown to improve antibacterial efficacy, inhibit biofilm formation, and lead to accelerated wound healing following infection with methicillin-resistant *Staphylococcus aureus*.

**Conclusion:** These data suggest that novel nanofibers could effectively shorten the wound-healing time by inhibiting biofilm formation, which make it promising candidates for treatment of MRSA-induced wound infections.

**Keywords:** nanofibers, wound enclosure, methicillin-resistant *Staphylococcus aureus*, biofilm, antibacterial effect

## Introduction

Multi-drug resistance has continued to increase. It is difficult to control wound infection formation and promote the healing using antibacterial drugs and wound dressings.[1] Wounds have an estimated healthcare cost of US$20 billions and pose a serious worldwide healthcare problem that affects millions of people.[2] Globally, wounds affect nearly 15% (8.2 million patients), and the estimated cost of treating such patients in 2018 was between $28.1 and $96.8 billion.[3] The high cost of wound dressings originates from the continuous demand for care products. In addition, the market for wound dressings is expected to grow by $15 billion to $22 billion in 2024.[4] The skin, including the epidermis and dermis, is the largest multi-layered organ in the body. The skin also acts as a protective barrier by preventing excessive water evaporation and protecting the body from pathogens.[5] However, once the skin is seriously damaged, it will lose its protective effects, especially in terms of resisting microbial infections at the local wound site will seriously delaying the healing process.[1] Wounds contaminated by bacterial infections can put patients at a high risk of death because bacterial biofilms form at the wound site; these biofilms protect the bacteria from antibacterial treatment and host immune responses.[6] A variety of antimicrobial agents, including polymyxin B sulfate, silver sulfadiazine, gentamicin, and bacitracin, for the treatment of wound infections are available.

Received: 1 July 2022
Accepted: 7 September 2022
Published: 21 September 2022

Meanwhile, these common topical forms, such as the ointments and gels, have little effect in practical application because they are easily removed from the exposed wound area.[7] The need to develop novel wound dressings to effectively absorb exudates, allow gas exchange, eliminate multi-drug bacterial infection, and promote the cell proliferation so as to accelerate the wound repair exists.[8] Modern wound dressings avoid re-injury of new granulation tissue due to scarring and promote the differentiation and migration of cell.[9,10] Wound dress polymers material that can be cross-linked with many materials include poly(vinyl pyrrolidone), poly(lactic-*co*-glycolic acid), poly(vinyl alcohol), polyurethanes, polyglycolic acid, polylactide, poly(hydroxyethyl methacrylate),[11] hyaluronic acid, chitosan, collagen, alginate, heparin, cellulose and bioactive peptide.[12] Although various advanced wound dressings have been developed and applied in the clinical setting, there is no relevant study investigating the reasonable selection of wound dressing.[13] Hence, development of a novel suitable wound dressing is vital for controlling the bacterial infection in the wound.

Methicillin-resistant *Staphylococcus aureus*, MRSA, is a serious threat to global health because of its high associated morbidity and mortality.[14] It is a common pathogenic and obstacle to wound healing. To make the situation worse, development of effective antibiotics for treating wound infections is a still worldwide problem.[15] In addition, the emergence of MRSA biofilms and persistent bacteria that are known to increase their antibiotic resistance has attracted more and more focus on these bacteria as a major human pathogen. However, no effective antimicrobial in clinical settings are available.[16] With the virulence of these pathogens and the widespread emergence of MRSA, an urgent need to find new ways to treat these infections is needed as growing antibiotic resistance is considered a major threat to public health.[17]

Previous research has shown that benzalkonium bromide, BZK, can inhibit the growth of MRSA. Recent results confirm that several formulations of BZK, such as nanoscale-films,[7] hydrogels, foams, sponges, and nanoparticles[18] could lead to an improvement in the antibacterial effect and wound heal of infection. However, these topical formulations still cannot completely eradicate the MRSA in the local wound because of a short period of action. Data suggest that BZK can remain at the wound for a long time and should be more effective than a topical formulation.[19] Also, no reports about nanofibers-coated BZK in wound healing have been published. Novel nanofibers of wound dressings may greatly enhance wound healing.

Novel nanofibers of wound dressings may enhance greatly the wound healing[20] because of larger volume ratio or specific surface area and high porosity. It is well known that nanofibers can produce an improvement in cell adhesion, cell proliferation, and cell differentiation.[21] A pentapeptide epitope IKVAV with a negative charge and composed of lysine, laminin, valine, isoleucine, and alanine has been widely used for wound healing.[22] Also, the nanofibers containing this epitope can promote cell outgrowth processes and suppress cell differentiation.[23] Importantly, IKAVA can selectively promote neuronal differentiation and cell adhesion and inhibit glial differentiation and adhesion.[24] Additionally, it can promote many cellular behaviors such as cell adhesion, cell survival, cell outgrowth, and angiogenesis.[25] It may also facilitate neural progenitor cell differentiation into neurons.[26] Moreover, another biomimetic peptide, arginine-glycine-aspartate, RGD, a component of extracellular matrix proteins, plays also a crucial role in regulating cell adhesion and specific binding to proteins of the transmembrane region.[27] RGD can also stimulate cell activity, and its incorporation into the biomaterial surface produces scaffolds that can accelerate wound healing.[28] Therefore, IKVAV and RGD are ideal biomimetic peptides for facilitating wound healing.

In this study, BZK was loaded successfully into a novel nanofibers prepared via the novel self-assembly technology based on the ideal characteristics of biomimetic peptides of IKVAV and RGD as shown in Figure 1. BZK's different drug-dependent loaded effects, including encapsulation efficacy, swelling ratio, and strength, were determined. Its release profile in wound fluid and its cytotoxicity were studied in vitro. Importantly, the antibacterial efficacy and inhibition of biofilm formation effect and wound healing in MRSA infections based on in vitro and in vivo assays were performed to confirm the improved healing capacity of the novel nanofibers compared to soluble water-based solutions after tissue toxicity results were obtained in vivo.

# Materials and Methods

## Materials

Polyvinyl alcohol, PVA (87.0–89.0% alcoholysis) was supplied from Shanghai Merck Biochemical Technology Co., LTD. Chitosan, CS (95% deacetylation, viscosity 100–200 mpa•s) was obtained from Shanghai McLean Biochemical Co., LTD., China. IKVAV (molecular weight 1351.6, 97.6%) and RGD (molecular weight 1,207.34, 97.5%) were provided by Shanghai Botai Biotechnology Co., LTD. MRSA252 strains were purchased from ATCC (USA).

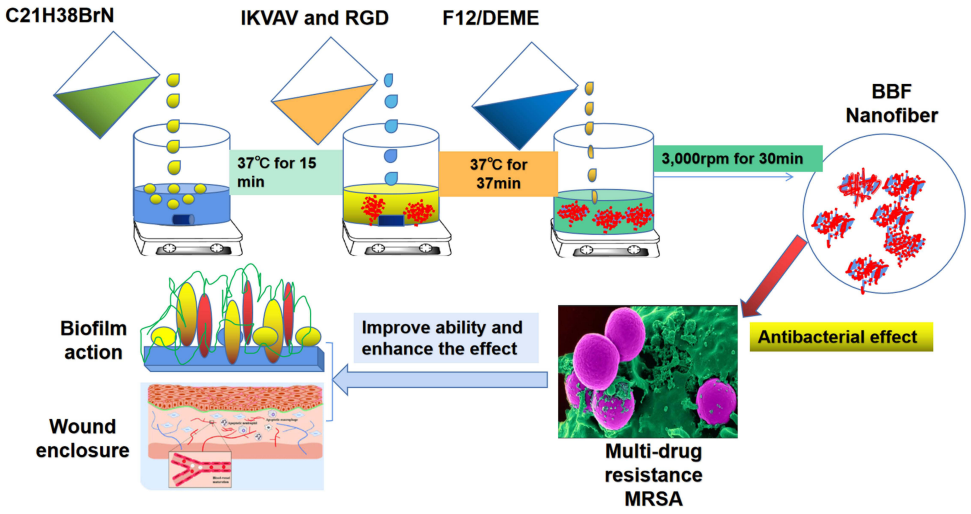


**Figure 1** Research schematic diagram of the novel bioactive antimicrobial nanofibers with benzalkonium bromide.
**Note**: This novel nanofibers (BBF) can effectively inhibit the antibacterial effect of multi-drug-resistant methicillin-resistant *Staphylococcus aureus* (MRSA) and enhance the capability of inhibiting biofilm formation, thereby accelerating wound healing.

Mueller–Hinton Broth (MHB), trypsin soybean broth (TSB), and Mueller–Hinton agar (MHA) were obtained from Beijing AOBOX Biotechnology (Beijing, China). BZK (50 mg/mL) was purchased from Yusheng Pharmaceutical (Chongqing, China), L929 cell line was purchased from the Cell Bank of Typical Cultures Preservation Committee, Chinese Academy of Sciences.

## Animals and Ethics Statement

BALB/c female mice (SPF grade, 6–8 weeks) were supplied from HFK Bioscience Co., Ltd. (Beijing, China). All mice were given aseptic water and autoclaved food at 23°C and 50% humidity with light and dark periods that each lasted 12 h in a quiet environment. Animal experiments were carried out after being approved by Animal Ethics and Experiment Committee of TMMU of Chinese PLA (Permit number No. 20170002, Chongqing, China) in accordance with the Guidelines for the Care and Use of Experimental Animals. To minimize pain, all mice that underwent surgery were anesthetized with 1% isoflurane and euthanatized with intraperitoneal injection of 100 mg/kg sodium pentobarbital.

## Preparation of BBF Antibacterial Nanofibers

Preparation of the nanofibers followed the procedure from a previous report.[24,29] Briefly, PVA, IKVAV, or RGD was added to a mixture of 0.1 M NaOH and distilled water. The mixture was then incubated at 37 °C for 30 min and stirred vigorously until a clear liquid was formed. The pH was measured and adjusted to a value of 8.5–9.0 with 0.1 M HCl. Then, BZK and chitons (pretreatment with 1% glacial acetic acid, v/v) were added to 0.1 mL Dulbecco's Modified Eagle Medium (DMEM)/F12 medium (Gibco, USA). Different concentrations of antibacterial nanofibers were thoroughly washed several times with deionized water to remove any residual NaOH.

## Different Drug Load Effects on the Nanofibers

The encapsulation efficiency was determined by dissolving six different drug content nanofiber (0, 0.1%, 0.2%, 0.4%, 0.8% and 1.6%, w/w) in absolute ethyl alcohol or distilled water based on methods by.[30] The mixture was then centrifuged at 8,000 ×*g* for 10 min, and the precipitate was resuspended in 1.2 mL distilled water. The encapsulation efficiencies of these samples after centrifugation (13,000 rpm, 20 min) were measured and calculated using high-performance liquid chromatography, HPLC,(NOA 280i, Agilent C18 column 5 μm, 4.6 mm×250 mm) with 0.07 mol/L ammonium acetate as mobile phase (1% triethylamine-acetonitrile, 30:70, pH 3.0 ± 0.1), wavelength set at 262 nm, flow rate (1.0 mL/min), and injection volume (10 μL). Encapsulation efficiency (EE %) = Actual content of total drug in the nanofibers/theoretical content of total drug loaded into the nanofibers×100%. Swelling ratio was detected by referring

to previously reported methods[31] Briefly, the swelling rate of the different drug concentration nanofibers in phosphate buffered saline (PBS, pH = 7.4) was studied by gravimetry. The initial dry weight of the sample was represented by *W*d. These samples were then immersed in PBS and placed in an incubator at 37 °C. Swollen samples were removed at different intervals. After removing excess water from the surface, the wet weight (Ww1) was measured. Swelling ratio (SR) (%) = (Ww1 –Wd)/Wws×100%, where Ww1 is the weight of swollen nanofibers and wd is the weight of dried nanofibers. Tensile strength was obtained as described in previous reports.[32] The tensile strength of these different drug content nanofibers (was measured using a Texture Analyzer (TA-XT2i, Micro-systems, UK) with preset conditions: (1) pressure sensor (5 kg, (2) tensile load (10 g), (3) fixture spacing (20 mm), and (4) test speed (5 mm/s).

## Micro-Structural, Size and Zeta Potential Measurements

The micro-structure of the novel nanofibers, BBF, was observed by a JEM-1230 transmission electron microscope, TEM (JEOL Limited Company, Japan) as previously reported.[24,33] TEM samples were diluted 200 times and then placed on the copper grid (PELCOL TEM 200-mesh) and dried under the grid cover for 10 min after which TEM observations were obtained after negative staining for 1 min with phosphotungstic acid solution (1% w/w, pH 7.4). Scanning electron microscopy, SEM, samples were diluted 100 times and observed using an S-3400N SEM at an acceleration 10 kV voltage and a sputter coating with gold palladium of 200 Å.[34] After diluting 200-fold with water, the average size and zeta potential of these nanofibers were measured using Nano ZS (Instruments Ltd., Malvern, UK).

## In vitro Release of These Novel Nanofibers in SWF

The release profiles of BBF and BZK were examined in simulated wound fluid, SWF, composed of 0.64% NaCl, 2.5% $NaHCO_3$, 0.22% KCl, and 0.35% $NaH_2PO_4$ at pH 7.4[35]. Briefly, 2 mL samples at 5 mg/mL drug concentration were added to a preprocessed dialysis bag of Sangon (cut-off molecular weight 10,000 g/mol, Shanghai, China) in 200 mL SWF. The drug concentrations were detected using HPLC for measuring the amount of compound released after 0, 0.25, 0.5, 0.75, 1, 2, 3, 6, 12, 24, 48, 96, and 192 h. Drug release ratio (%) = The amount of solubilized drug in the release medium//Initial weight of the entrapped drug)×100%.

## In vitro Biocompatibility in the L929 Cell Line

Cell studies were conducted using the L929 cell line to evaluate the biocompatibility of these nanofibers. Using a biopsy perforator, the nanofibers were cut into circles of 1 cm in diameter and attached to the bottom of 24-well culture plates. Prior to cell culturing, the nanofiber wells were pretreated with DEME complete medium (10% FBS, 1% penicillin/streptomycin) and placed in the 5% $CO_2$ incubator at 37 °C for 24 h. The media were then refreshed, and the cells with $3\times10^5$ cells/well were mixed with the nanofibers at nanofiber concentrations of 200, 100, 50, 25, 12.5, 6.25, and 3.125 μg/mL. The CCK8 (10 μL) solution was added to each well, and cells were incubated at 37 °C for 4 h. These samples were measured by Microplate Reader at 490 nm. Cell viability (%) = [(As-Ab)/(Ac-Ab)] × 100%, where As is the absorbance of the experimental well, Ab is the blank well absorbance, and Ac is the control well absorbance.

## Antibacterial Against Multi-Drug MRSA in vitro

Antibacterial activity against multi-drug MRSA was evaluated using the micro-dilution and agar plate methods described previously to determine minimum inhibitory and minimum bactericidal concentrations (MIC and MBC, respectively) in vitro.[18] Briefly, BBF were diluted to 5.0, 10.0, 20.0, 40.0, 80.0, 160, 320, or 640 μg/mL, and 20 μL of each suspension was mixed with 180 μL of MRSA 252 suspension ($1.0 \times 10^5$ colony-forming units [CFU]/mL) in 96-well plates (Costar 3599, Corning Inc., NY, USA) at 37°C for 24 h. Optical density, OD, was read at 595 nm using a Bio-Rad 6.0 microplate reader. The MIC was considered the lowest concentration that indicated $OD_{595}$ nm value $<0.05^7$. MIC bacterial solution (2 μL) per well was added to the BHI agar plate and incubated at 37°C for 16 h after which the colonies were observed with the naked eye. The MBC represents the minimum concentration of nanofibers required to achieve a 99.9% reduction in colony forming units, CFU. Bacterial cultures ($1 \times 10^7$ CFU/mL) were incubated in BBF and BZK at concentrations of 4.0 and 2.0 μg/mL, respectively, for 0, 0.0167, 0.0833, 0.25, 0.5, 0.75, 1, 2, 4, and 8 h. After the incubation period, 2 μL of samples were diluted 10-fold (0, $10^1$, $10^2$, $10^3$, $10^4$, $10^5$, and $10^6$) with MHB, added to MHA plates, and incubated at

37°C for 24 h. Bacterial numbers on the plates were counted with an automated colony counter (Shineso Science & Technology Co., Ltd, Hangzhou, China).

## Biofilm Inhibitory Effects of the Novel Nanofibers

BZK and BBF (0.2 mL each, both containing 2.0 μg/mL) were added to a MRSA bacterial suspension (1.8 mL, $1\times10^7$ CFU/mL) into each well of a 24-well plate with coverslips (Thermo, Rochester, USA). The bacterial cultures were incubated (37 °C, 24 h) and washed twice with 0.1 M sterile PBS. After removal of the supernatant, the wells were washed twice with 1 mL of physiological saline and fixed with 1 mL absolute ethanol for 15 min and stained for 10 min with 200 μL 0.1% crystal violet, CV, dye. Thirty percent (1 mL) acetic acid was added to each well after washing twice with physiological saline. The OD at 595 nm was measured with a Bio-Rad 6.0 Microplate reader (Bio-Rad Laboratories Inc., CA, USA). Additionally, after removal of the supernatant, the coverslip samples were fixed with 2.5% glutaraldehyde. These samples were processed for SEM observation after treatment through an ethanol concentration gradient. The samples were observed by an S-3400N SEM (Hitachi, Japan) with an accelerating voltage (10 kV) and a sputter (200 Å) coating of gold-palladium.

## In vivo Accumulative Toxicity Assays

In vivo experiments were performed under the guidelines of the Animal Ethics Committee of the Army Medical University. The six mice (BALB/C) were divided randomly into two groups: (1) BZK aqueous solution (5 mg/mL) and (2) its nanofibers (5 mg/mL). Briefly, mice were anesthetized via intraperitoneal injection with ketamine and xylazine. The surgical sites of the mice were shaved and then disinfected with 75% ethanol. The mice were also treated with 50 μL of the drug solutions daily for 10s for 14 days. After treatment, all mice were sacrificed, and hearts, livers, spleens, lungs, kidneys, and skin tissues were fixed with 4% paraformaldehyde for 24 h and then embedded in paraffin. After the samples were stained with hematoxylin and eosin, H&E, the toxic effects in the tissues were examined with an Olympus light microscope.

## In vivo Acceleration of Wound Healing

In vivo acceleration of wound healing was also performed under the guidelines of the Animal Ethics Committee of the Army Medical University. Briefly, mice were treated with intraperitoneal injections of ketamine and xylazine. The surgical sites were shaved and disinfected with 75% ethanol. Thirty mice were divided randomly into five groups: (1) nanofibers (5 mg/mL) and (2) corresponding aqueous solution (5 mg/mL), (3) blank nanofiber control, BNF, (4) vancomycin group (5 mg/mL), and (5) wound infection control group after creating 1 cm × 1 cm square full-thickness skin wounds. Also, the wound skin was treated with 50 μL of sample daily for 5 s. For wound closure assessments, photographs of the wound area were taken on post-operative days 7 and 14. On days 1, 4, 7, 10, and 14, wound areas (lengths and widths) were measured using ImageJ software, and the wound closure percentage was obtained. Wound healing rate (%)= [(At=0 h – At =Δ h)/At= 0h]×100%, where At=0h is the area of wound measured immediately and At=Δh is the area of wound measured after different times.

## Reduction of Bacterial Burden in the Local Wound

The bacterial load in the local wound was determined on post-treatment day 7. Swabs were separated from the wound and placed in 1 mL of sterile 0.9% NaCl as previously described.[36] The swabs were swirled to release the bacteria into the solutions and then continuously diluted six times with 10-fold sterile saline after which 2 μL of the diluted samples were added to the MHA plate and incubated at 37°C for 24 h. After incubation, the bacterial colonies were counted with an automatic colony counter (Shineso Science & Technology Co., Ltd, Hangzhou, China).

## Histological Properties

To assess the histological properties of each group on day 7, the regenerated wound tissue was taken and fixed for 24 h with 10% formalin solution. These samples were then dehydrated, cleared, paraffinized, and embedded in stages and then

sliced using a microtome to obtain tissue sections of 5 μm thickness. The slides were photographed using a light microscope (Nikon) after staining with hematoxylin–eosin staining.

### Statistical Analysis

Statistical differences were obtained by GraphPrism 8.0 software using one-way analysis of variance (ANOVA). All results were shown as mean ± standard deviation (SD), and $P < 0.05$ was considered statistically significant.

## Result and Discussion

### Preparation of the Novel Antibacterial Nanofibers

In this study, the novel antibacterial nanofibers containing BZK were prepared based on the previously described methods.[24] Additionally, IKVAV and RGD bioactive peptides were synthesized separately by Shanghai Botai Biotechnology Co., Ltd, and the nanofiber scaffolds were developed using the self-assembly technology of electrostatic and hydrophobic interactions. Our results indicate that the optimal ratio (IKVAV:RGD) of nanofibers was 3:1 determined by observing its flow capability, diffusivity, and viscosity and the corresponding drug concentrations were 1, 2, 4, and 8 mg/mL. Many studies have reported that IKVAV and RGD are selected for nanofiber development because these peptide-functionalized substrates can enhance cellular behavior. In particular, these peptide-conjugated substrates based on multiple biocompatible materials, such as polycaprolactone, chitosan, poly(L-lactide), and polystyrene have been widely applied for tissue engineering scaffolds.[37,38] Moreover, the nanofibers are composed of the bioactive peptides IKVAV; these peptides on the outermost surface directly affect cell adhesion.[39] Therefore, IKVAV/RGD was chosen to enhance the adherence efficiency of bioactive peptides on the surface of the novel nanofibers.

### Different Drug Concentration Effects on the Nanofibers

The effects of different drug concentrations in the nanofibers on encapsulation efficacy, swelling ratio, and stress are shown in Figure 2A–C. According to Figure 2A, with increasing drug concentration from 0% to 0.8% (8000μg/mL), the encapsulation efficiency increases up to 92.56% and then (1.6%) decreased abruptly ($P<0.01$). These data show that at 8000 μg/mL, swelling changed from 0.73 ± 0.015 to 0.63 ± 0.014 ($P < 0.001$) as shown in Figure 2B. In addition, the tensile strength of BBF changed from 75 ± 6.48 mV to 182 ± 0.51 MPa, but a significant difference ($P < 0.05$) was found under the concentration of 8000 μg/mL (Figure 2C). In our study, the three main indicators of encapsulation efficiency, swelling degree, and tensile strength were chosen for several reasons: (1) encapsulation efficiency represents the amount of drug incorporated into nanofibers, which is important and useful to materials.[40] In this study, the highest encapsulation efficiency of 92.55% was obtained when the drug concentration was 8000 μg/mL. It is believed that the ideal encapsulation efficiency will be attributed to drug delivery in nanofibers rather than through aqueous solutions. Furthermore, the expansion efficiency of scaffolds plays a crucial role in tissue engineering applications as it facilitates the exchange of cellular metabolites and nutrients. The expansion potential of the developed nanofiber scaffolds was tested under aqueous conditions at room temperature, and the results are shown in Figure 2B. These data indicate that BBF at a drug concentration of 8000 μg/mL had higher swelling efficacy than the other groups, indicating that this concentration was optimal as shown in Figure 2C. (2) The high swelling capacity of the nanofibers increases the contact of the fibers with the wound site during topical administration. Consequently, nanofibers are easily distributed within mucosal structures and active substances are released through the skin.[41] These results show that ideal nanofibers were obtained, and (3) tensile stress is an important parameter for designing and developing nanofiber structures.[42] In this study, it was found that the nanofibers had higher tensile strength when compared with other drug concentrations, which confirmed the feasibility of our model. These data suggest that a BBF with an optimized drug concentration of 8000 μg/mL would be ideal for our studies.

### Morphological and Basic Characteristic of the Nanofibers

The morphological and basic characteristics of the resulting nanofibers were observed by TEM, SEM, and dynamic light scattering (DLS) as shown in Figure 3A–F. These results suggested that the novel nanofibers had a fibrous appearance

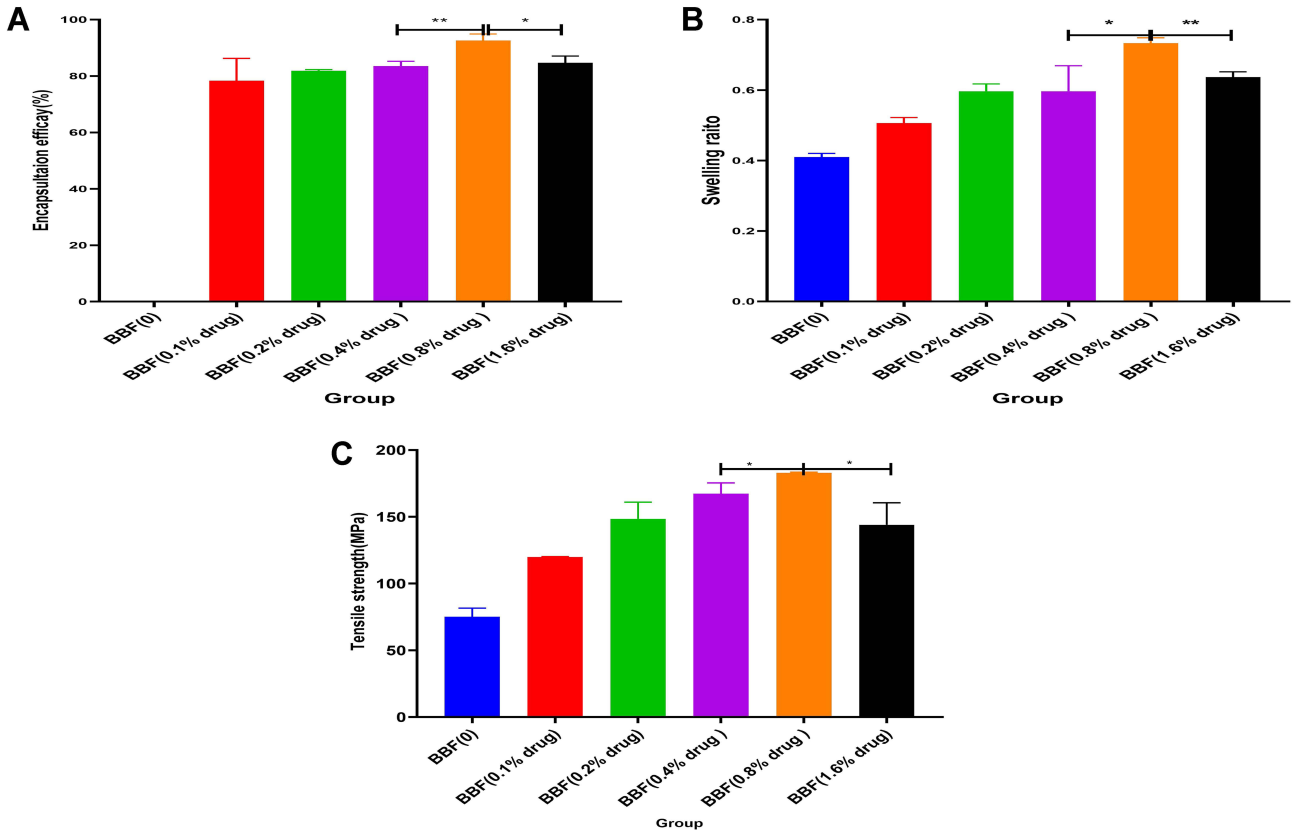


**Figure 2** Effects of six different drug loading on the encapsulation efficiency (**A**), swelling ratio (**B**) and tensile strength (**C**).
**Notes**: *$P < 0.05$ is a difference, **$P < 0.01$ is a significant difference. Error bars represent the mean ± standard deviation (n=3).

under the two different magnifications. With a magnification of 45,000× (Figure 3A), the nanofibers were found to be more homogeneously dispersed. However, at a magnification of 65,000× (Figure 3B), the nanofibers could be directly observed. SEM images of the novel nanofibers (Figure 3C and D), with magnifications of 15,000× and 30,000× yielded clear images of nanofibers morphology. This morphology of the BBF nanofibers was similar to cellulose and chitin nanofibers that were obtained by mechanical grinding.[42]

Hence, the excellent dispersion in water indicates that the nanofibers were successfully loaded with BZK. Figure 3E shows that the particle size of BBF at 8000 μg/mL was mostly around 220 nm, and one peak is observed, with the main peak at 220.0 nm. In addition, the pH was 6.52, the conductivity was 0.244 mS/cm, and the electrophoresis mobility was −1.442 μmcm/Vs. The narrow polydispersity index (PDI) of 0.199 indicated a high and good degree of size distribution. The zeta potential with a BBF of −11.2 mV (Figure 2F) indicated moderate stability with no tendency to self-aggregate in colloidal suspension. Overall, these BBFs have stable negative zeta potentials.

## In vitro Release in the Simulated Wound Fluid

In vitro release profiles were HPLC, which is a sensitive and accurate detection method. Results indicated that nanofibers had a delayed release in SWF fluid (Figure 4A). A significant difference between BBF and its aqueous solution at 24 h ($P = 0.0001$ and $P < 0.001$, respectively) was found; the release rate of its aqueous solution was as high as 90%, while that of BBF was less than 30%. In conclusion, relative to its aqueous solution, BBF does not immediately disintegrate or release active drug through the skin into the subcutaneous tissue fluid; therefore, BBF exhibits a significantly sustained release. Many factors affect drug release from nanofibers, including the type of polymer used to form nanofibers, its diameter, morphology, porosity, and geometry, have been reported.[43] Therefore, it is believed that water molecules can also penetrate the nanofibers; thus, a large number of drugs can be released slowly, mainly because of the barrier effect of

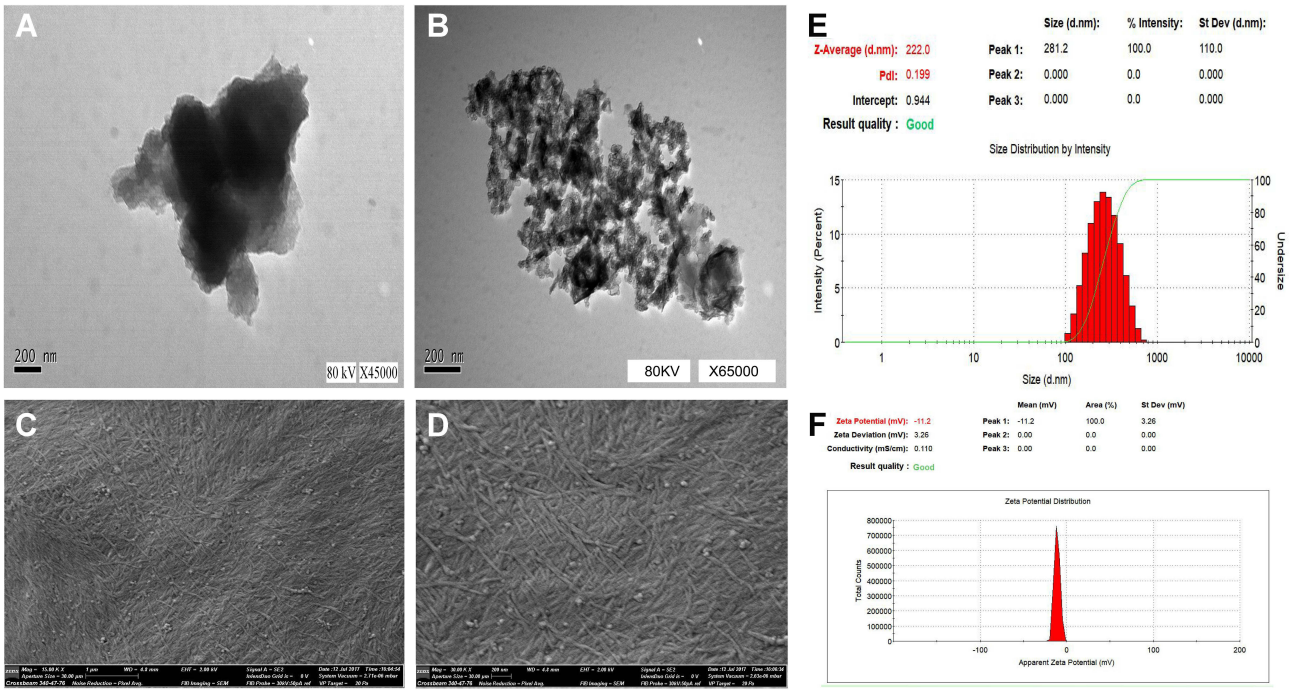


**Figure 3** Morphological and physicochemical characteristics of the nanofibers. (**A**) Transmission electron microscopy morphological image (45,000× magnification), (**B**) transmission electron microscopy morphological image (65,000× magnification), (**C**) scanning electron microscopy morphological image (15,000× magnification), (**D**) scanning electron microscopy morphological image (30,000× magnification), (**E**) the diameter distribution, (**F**) zeta potential distribution.

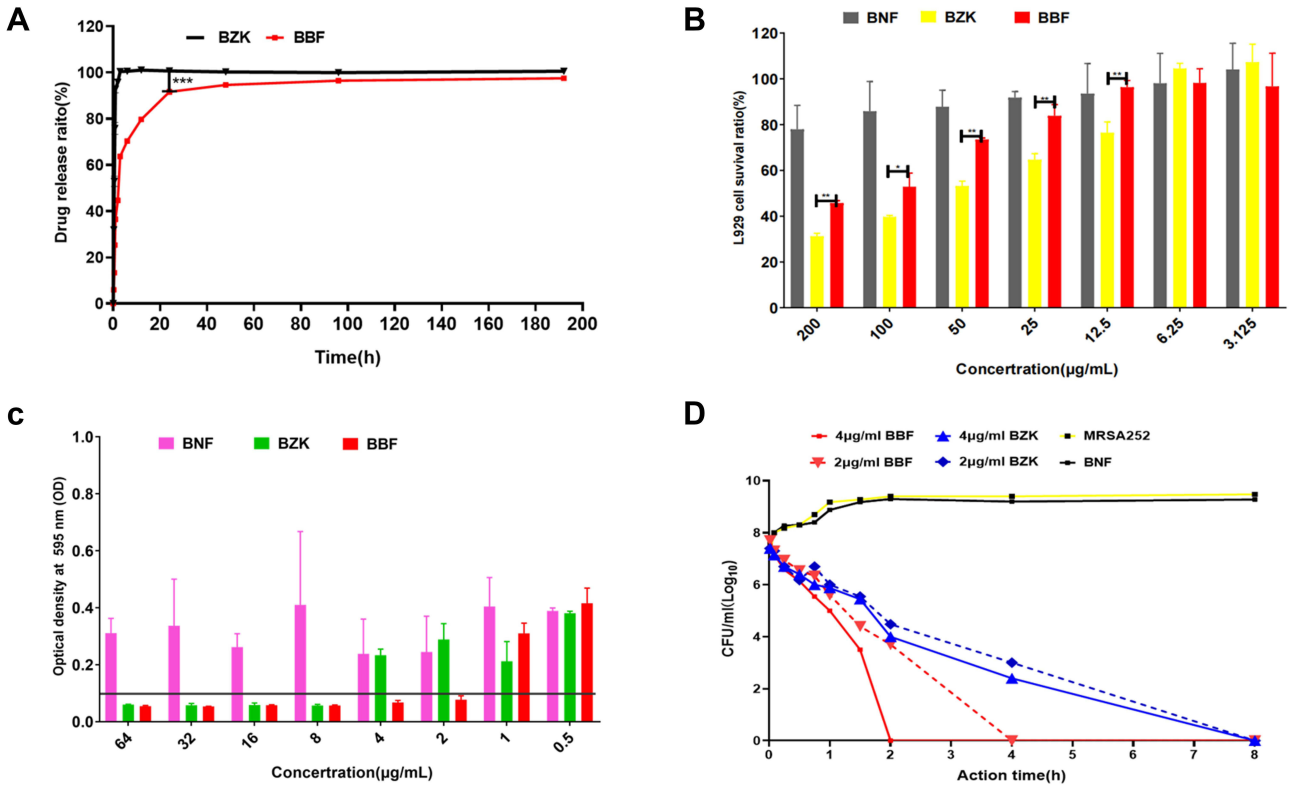


**Figure 4** Release profile, cytotoxicity, and antimicrobial activity of the novel nanofibers. (**A**) In vitro release profiles. (**B**) In vitro L929 cytotoxicity. (**C**) Minimum inhibitory concentration. (**D**) Time-kill analysis.

**Notes**: *$P < 0.05$ is a significant difference, **$P < 0.01$ is a highly significant difference and ***$P < 0.001$ is an extremely significant difference. Error bars represent the mean ± standard deviation (n=3).

the nanofibers.[44] In this study, the resulting novel nanofibers were shown to achieve a continuous and delayed release in the SWF.

## In vitro Biocompatibility

Biocompatibility of the novel nanofibers is one of the fundamental requirements for the manufacture of wound dressings. The biocompatibility of nanofibers was assessed using L929 fibroblasts. In Figure 4B, the cell viability assay showed that cell proliferation was linear with concentration reduction. After culturing, the proliferation rate of cells in the control group was higher than that in the other groups, except at the concentrations of 3.125 and 6.25 μg/mL. The difference was statistically significant (all $P<0.05$). This result could be attributed to the flat, cell-adhesion conductive medium, which facilitates simple and efficient cell attachment, cell signaling, and cell proliferation.[45] Furthermore, studies have shown that at high cell densities, the pore spaces in the scaffolds fill rapidly, resulting in reduced proliferation because cell contact inhibition growth.[45] CCK8 results demonstrated that nanofibers can help maintain cells and provide the appropriate growth environment for fibroblasts. In the process of wound healing, fibroblast migration from various sources contributes to the formation of granulation tissue and extracellular matrix, which is very important for wound healing.[9] These results indicate that the novel nanofibers exhibit good biocompatibility.

## In vitro Antibacterial Test

In this regard, the MICs of nanofibers were determined in terms of MRSA252 as shown in Figure 4C. The MIC and MBC of the nanofibers and their corresponding water solutions with BZK were 1 and 4 μg/mL, respectively, which was consistent with previous findings.[7,18] Furthermore, MBC of 1 and 4 μg/mL was required to kill bacterial cells after treatment with BBF and its corresponding aqueous solution. These data indicate that BBF can lead to an improvement in antibacterial effects against MRSA. The results of time-dependent killing showed that BBF at 2 and 4 μg/mL both exhibited faster and more effective anti-bactericidal activity than BZK at the same concentration; the killing of MRSA 252 was a time- and concentration-dependent relationship as shown in Figure 4D. At 4 μg/mL BBF, these bacteria were killed completely in about 120 min, whereas in contrast, BZK-treated bacteria, which resulted in 75% bacterial death, were not completely killed within the same time period. At 2 μg/mL BBF, the bacteria were killed completely in about 240 min; however, the same concentration of BZK could not completely kill the bacteria within the same periods. Moreover, it was found that BNF had no obvious inhibitory effects on bacterial viability. Bacterial infection is one of the main obstacles to wound healing and can prolong the healing process. Therefore, it is necessary to study the antibacterial capability of novel nanofibers. In our study, MIC, MBC, and time-kill kinetic assays were used to evaluate the antibacterial properties of nanofibers against MRSA. Our data confirm that BBF has stronger and more potent bactericidal activity than its aqueous solution.

## In vitro Inhibit Biofilm Formation Activity

Crystal violet staining was used to the quantitatively assess the biofilm formation of the novel nanofibers. The $OD_{570nm}$ values of the biofilm samples treated with BZK and BBF aqueous solutions were 2.231 ± 0.118 and 0.663 ± 0.123, respectively, indicating a 3.36-fold reduction in the biofilm formation of their nanofibers after treatment for 24 h. In Figure 5, MRSA was treated for 24 h with a 2 μg/mL BBF followed by an SEM analysis for physical and morphological changes. Biofilms in bacteria treated with nanofibers were viewed at 2,000× and 8,000× magnifications (Figure 5A and D) and found to be diffused and disrupted, and the numbers of bacteria present were significantly reduced. SEM images of bacteria treated with BZK water solution (Figure 5B and E) showed similar morphology to the BNF control (Figure 5C and F). It can be observed in the images that the thickness of the nanofibers of the bacterial cell clusters were much smaller than that of the nanofibers exposed to the same concentration of aqueous solution. It is well known that biofilm formation causes the inflammation that hinders the wound healing process.[43] Meanwhile, a variety of MRSA-persistent bacterial cells with lower antimicrobial activity were embedded in the biofilm.[44] Therefore, the nanofibers with anti-biofilm inhibition show the capability of controlling and improving wound healing.

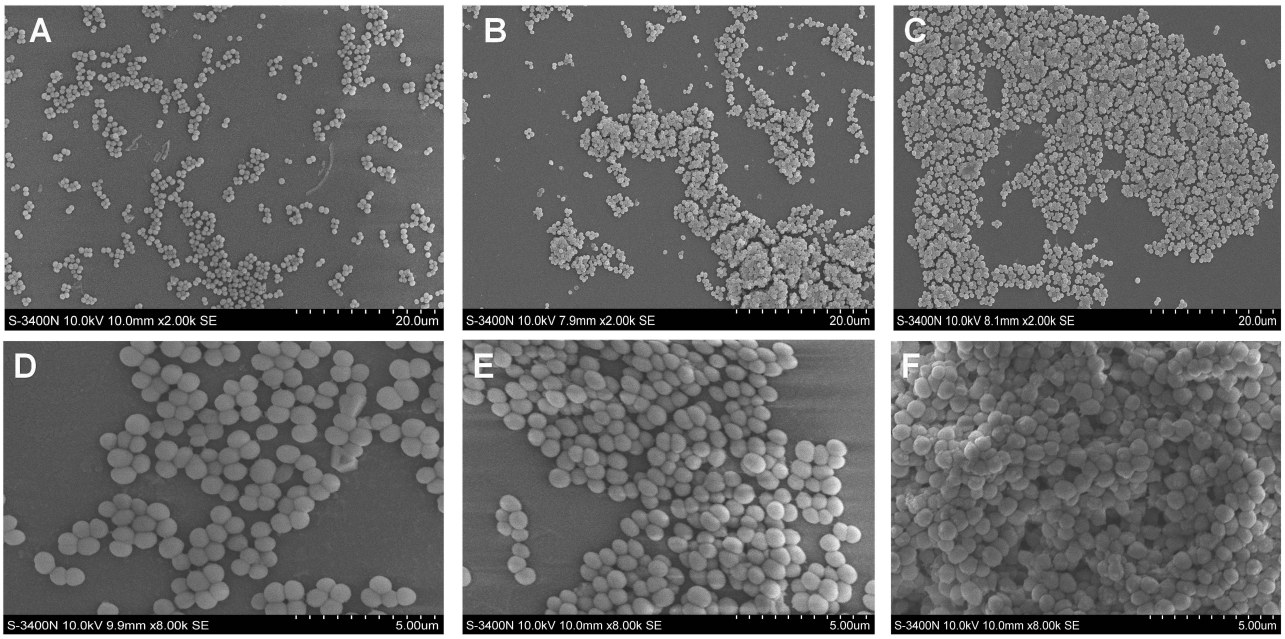


**Figure 5** Surface structure of inhibited biofilm formation observed by SEM. (**A**) 1 μg/mL novel nanofibers, BBF, treatment group (2,000× magnification). (**B**) 1 μg/mL benzalkonium bromide treatment group (2,000× magnification). (**C**) Blank nanofibers, BNF, control (2,000× magnification). (**D**) 1 μg/mL novel nanofibers, BBF, treatment group (8,000× magnification). (**E**) 1 μg/mL BZK treatment group (8,000× magnification). (**F**) Blank nanofibers, BNF, control (8,000× magnification).

## In vivo Toxicity of the Nanofibers

The nanofibers cytotoxicity in L929 cells was measured using CCK8 assay. It was demonstrated that the nanofibers did not cause significant cell cytotoxicity. In vivo nanofibers toxicity, as shown in Figure 6, the histological examination showed that the hearts, livers, spleens, lungs, kidneys, and skin of all groups of mice presented no obvious cellular infiltration into the alveolar and interstitial spaces of the tissue. That is, no apparent inflammatory cell infiltration; hemorrhaging or tissue damage could be observed in the major tissues. The toxicity of BZK has been reported, but BZK cannot be added to food. It remains on the food contact surface at high concentrations (≥2000 μg/mL). It is imperative to

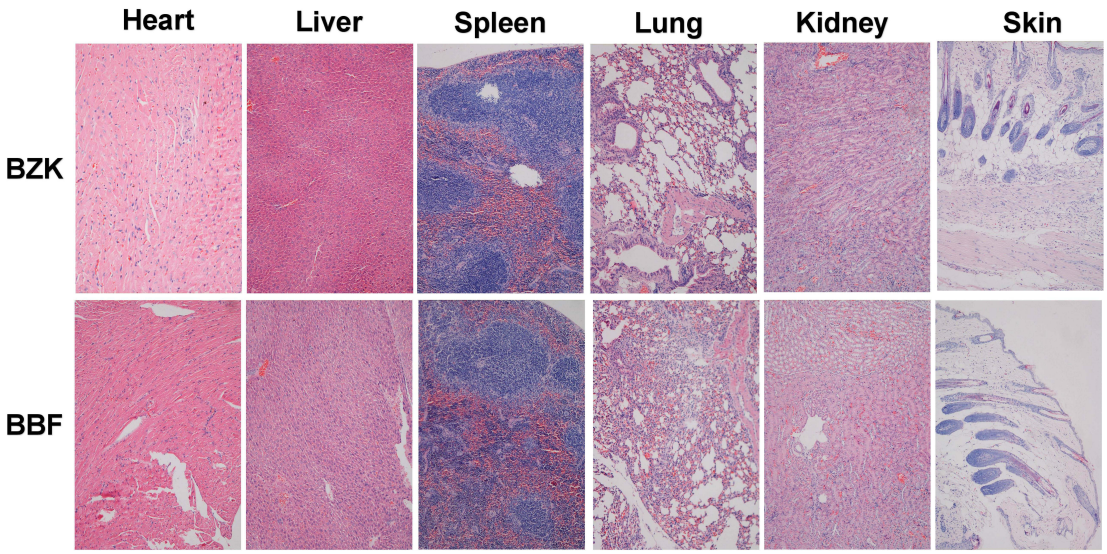


**Figure 6** Histotoxicity images of the novel nanofibers (BBFs).
**Note**: Histological microscope images of the hearts, livers, spleens, lungs, kidneys, and skin after 7 days of treatment with BZK aqueous solution and its nanofibers (BBF) in mouse skin irritation (100× magnification, scale bar: 100 μm).

ensure that BZK is thoroughly flushed from the system and that this concentrations on food contact surfaces must be tested prior to food processing.[12] Therefore, these novel nanofibers can be safely used in animal experiments and could become a potential biomaterial for biomedical applications and wound skin tissue engineering.

## In vivo Wound Healing Study

Given the excellent performance of BZK, the promotion of wound healing by nanofibers in vivo through a wound mouse model of infected MRSA was examined. Bacterial counts in local wounds treated with 5 mg/mL were determined. BBF decreased more rapidly than those of the same concentration of BZK after 7 days (Figure 7A). Complete clearance of bacterial counts in wounds locals in mice treated with 5 mg/mL BBF was detected, whereas wounds treated with BZK had a 57% reduction in bacterial counts. These data indicate that BBF led to significant killing of MRSA bacteria. In this study, a mouse skin full-thickness defect model that was infected with MRSA was used to evaluate the efficacy of the nanofibers to accelerate wound healing. Figure 7B and C shows macroscopic optical images and quantitative assessment of wound shrinkage in different experimental groups, including wound with infection control, BZK, BBF, vancomycin, and BNF controls (days 7 and 14). Quantitative assessment of wound healing showed that after 5 days of treatment, wound closure was similar between the experimental groups and was not significantly different. On day 10, the rate of wound shrinkage in the BBF group (about 45.1%) was significantly higher ($P < 0.01$). This result indicates that BBF is more effective in promoting wound healing. After 14 days of wound induction, the wound shrinkage rate in the BBF experimental group was higher (about 99.2%), and the difference between the groups was more significant. These results suggest that BBF also accelerated better wound healing performance than the other groups. Histological examination was performed to further evaluate the wound healing process. The wound healing effect of the dressing was assessed by performing hematoxylin and eosin as shown in Figure 7C. Wound infections of MRSA controls and BNF exhibited severe inflammatory responses. Wounds treated with 5 mg/mL BBF exhibited mild inflammation, and the skin could be separated into three distinct layers. In contrast, wounds treated with 5 mg/mL BZK exhibited the same severe inflammatory response as the group without treatment, and the skin tissue exhibited severe damage. These results suggest that BBF is more effective in healing MRSA-infected skin wounds than BZK.

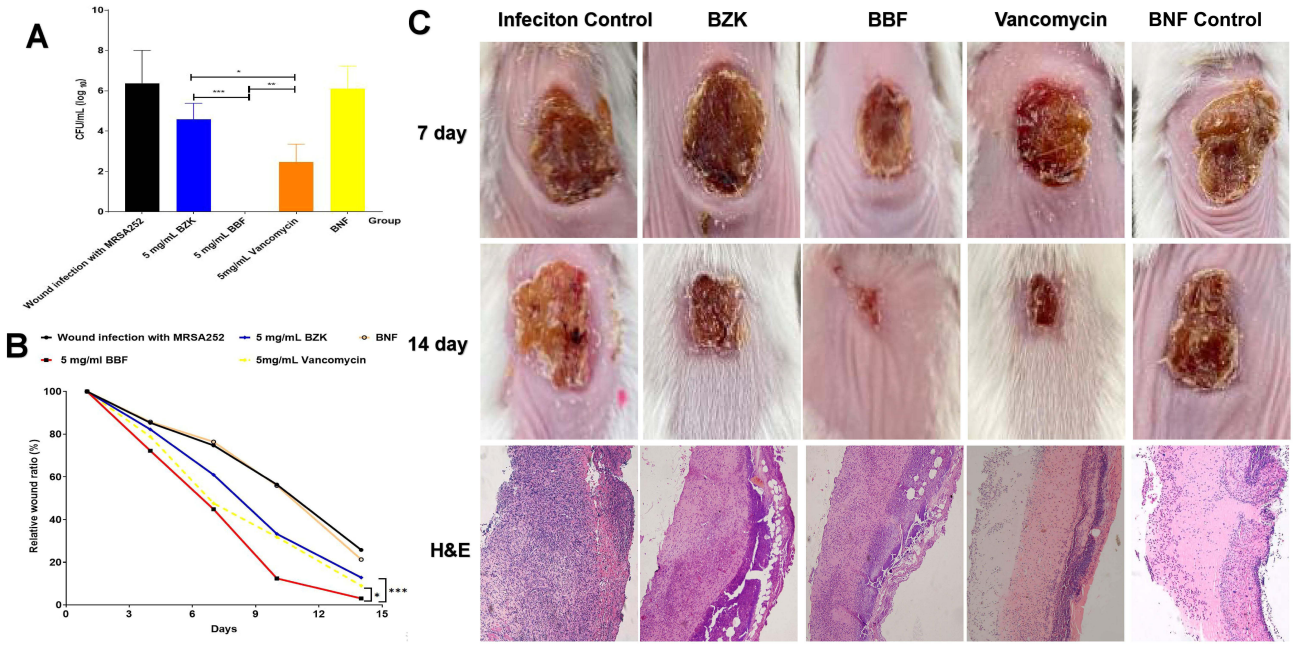


**Figure 7** Antibacterial activity and wound closure against MRSA infection in vivo. (**A**) Bacterial burden on days 7 after wounding; (**B**) relative healing area ratio of wounds. (**C**) Histological microscopy images of untreated wounds and infections treated with BZK aqueous solution, BBF, vancomycin control, and blank nanofibers (BNF).
**Notes**: Wound image (scale bar, 1 cm) and histological microscope (100× magnification, scale bar: 100 μm). *$P < 0.05$ is a difference, **$P < 0.01$ is a significant difference and ***$P < 0.001$ is an extremely significant difference. Error bars represent the mean ± standard deviation of each experiment (n=6).

## Conclusion

In this study, the novel self-assembled nanofibers of benzalkonium bromide with IKVAV and RGD bioactive peptide were designed and fabricated. Then, we found that the optimized drug load (0.8%) was affected by the encapsulation efficacy, swelling ratio, and strength. In addition, the novel nanofibers with average diameter (222.0 nm) and stabile zeta potential (−11.2 mV) have good morphology and characteristics. This nanofiber had not only a delayed released profile in the simulated wound fluid but also good biocompatibility with L929 cells in vitro, and no significant tissue toxicity including the liver, heart, spleen, kidney, lung and skin after skin irritation was administered compared with its water solution. Furthermore, the novel nanofibers exhibited significant antibacterial activity against methicillin-resistant *Staphylococcus aureus* and improved the capability of inhibiting biofilm formation in vitro. Importantly, our findings indicate that treatment with BBF could lead to a reduction in bacterial burden in the wound and accelerate wound healing in the current wound healing model with MRSA. These data suggest that novel nanofibers are an ideal therapeutic substitute for the wound infection with multi-drug-resistant bacteria.

## Abbreviation

IKVAV, isoleucine-lysine-valine-alanine-valine; MRSA, methicillin-resistant *Staphylococcus aureus*; BZK, benzalkonium bromide; RGD, arginine-glycine-aspartate; PVA, polyvinyl alcohol; CS, chitosan; MHB, Mueller–Hinton broth (MHB); TSB, trypsin soybean broth; MHA, Mueller–Hinton agar; HPLC, high-performance liquid chromatography; PBS, phosphate-buffered saline; TEM, transmission electron microscope; SEM, scanning electron microscopy; SWF, simulated wound fluid; DEME, Dulbecco's Modified Eagle Medium; MIC, minimum inhibitory; MBC, minimum bactericidal concentrations; CFU, colony-forming units; DLS dynamic light scattering; BBF, benzalkonium bromide nanofibers; BNF, blank nanofibers; PDI, polydispersity index; CV, crystal violet.

## Acknowledgment

The research was supported by the Natural Science Foundation of Chongqing cstc2018jcyjAX0222. We also thank Charles worth Author Services for language assistance during the preparation of this manuscript.

## Disclosure

The authors report no conflicts of interest in this work.

## References

1. Yang Y, Liang Y, Chen J, Duan X, Guo B. Mussel-inspired adhesive antioxidant antibacterial hemostatic composite hydrogel wound dressing via photo-polymerization for infected skin wound healing. *Bioact Mater*. 2022;8:341–354. doi:10.1016/j.bioactmat.2021.06.014
2. Thapa RK, Winther-Larsen HC, Ovchinnikov K, Carlsen H, Diep DB, Tonnesen HH. Hybrid hydrogels for bacteriocin delivery to infected wounds. *Eur J Pharm Sci*. 2021;166:105990, 1-10. doi:10.1016/j.ejps.2021.105990
3. Sen CK. Human wounds and its burden: an updated compendium of estimates. *Adv Wound Care*. 2019;8(2):39–48. doi:10.1089/wound.2019.0946
4. Kamoun EA, Loutfy SA, Hussein Y, Kenawy ES. Recent advances in PVA-polysaccharide based hydrogels and electrospun nanofibers in biomedical applications: a review. *Int J Biol Macromol*. 2021;187:755–768. doi:10.1016/j.ijbiomac.2021.08.002
5. Li M, Liang Y, He J, Zhang H, Guo B. Two-pronged strategy of biomechanically active and biochemically multifunctional hydrogel wound dressing to accelerate wound closure and wound healing. *Chem Mater*. 2020;32(23):9937–9953. doi:10.1021/acs.chemmater.0c02823
6. Li M, Li N, Qiu W, et al. Phenylalanine-based poly(ester urea)s composite films with nitric oxide-releasing capability for anti-biofilm and infected wound healing applications. *J Colloid Interface Sci*. 2022;607(Pt 2):1849–1863. doi:10.1016/j.jcis.2021.10.016
7. Yang S, Yang Y, Cui S, et al. Chitosan-polyvinyl alcohol nanoscale liquid film-forming system facilitates MRSA-infected wound healing by enhancing antibacterial and antibiofilm properties. *Int J Nanomedicine*. 2018;13:4987–5002. doi:10.2147/IJN.S161680
8. Huang Y, Bai L, Yang Y, Yin Z, Guo B. Biodegradable gelatin/silver nanoparticle composite cryogel with excellent antibacterial and antibiofilm activity and hemostasis for Pseudomonas aeruginosa-infected burn wound healing. *J Colloid Interface Sci*. 2022;608(Pt 3):2278–2289. doi:10.1016/j.jcis.2021.10.131
9. Shi C, Wang C, Liu H, et al. Selection of appropriate wound dressing for various wounds. *Front Bioeng Biotechnol*. 2020;8:182, 1-17. doi:10.3389/fbioe.2020.00182
10. Stoica AE, Chircov C, Grumezescu AM. Nanomaterials for wound dressings: an up-to-date overview. *Molecules*. 2020;25(11):2699, 1-25. doi:10.3390/molecules25112699
11. Alven S, Peter S, Mbese Z, Aderibigbe BA. Polymer-based wound dressing materials loaded with bioactive agents: potential materials for the treatment of diabetic wounds. *Polymers*. 2022;14(4):724, 1-35. doi:10.3390/polym14040724
12. Guan T, Li J, Chen C, Liu Y. Self-assembling peptide-based hydrogels for wound tissue repair. *Adv Sci*. 2022;9(10):e2104165, 1-26. doi:10.1002/advs.202104165

13. Powers JG, Higham C, Broussard K, Phillips TJ. Wound healing and treating wounds: chronic wound care and management. *J Am Acad Dermatol*. 2016;74(4):607–25. doi:10.1016/j.jaad.2015.08.070
14. Xie J, Zhou M, Qian Y, et al. Addressing MRSA infection and antibacterial resistance with peptoid polymers. *Nat Commun*. 2021;12(1):5898, 1-13. doi:10.1038/s41467-021-26221-y
15. Xu S, Chang L, Hu Y, et al. Tea polyphenol modified, photothermal responsive and ROS generative black phosphorus quantum dots as nanoplatforms for promoting MRSA infected wounds healing in diabetic rats. *J Nanobiotechnology*. 2021;19(1):1-20. doi:10.1186/s12951-021-01106-w
16. Liu Y, She P, Xu L, et al. Antimicrobial, antibiofilm, and anti-persister activities of penfluridol against Staphylococcus aureus. *Front Microbiol*. 2021;12:727692, 1-15. doi:10.3389/fmicb.2021.727692
17. Gandra S, Alvarez-Uria G, Turner P, Joshi J, Limmathurotsakul D, van Doorn HR. Antimicrobial resistance surveillance in low- and middle-income countries: progress and challenges in eight South Asian and Southeast Asian countries. *Clin Microbiol Rev*. 2020;33(3):1-29. doi:10.1128/CMR.00048-19
18. Wu D, Wei D, Du M, Ming S, Ding Q, Tan R. Targeting antibacterial effect and promoting of skin wound healing after infected with methicillin-resistant Staphylococcus aureus for the novel polyvinyl alcohol nanoparticles. *Int J Nanomedicine*. 2021;16:4031–4044. doi:10.2147/IJN.S303529
19. Alabresm A, Chen YP, Wichter-Chandler S, Lead J, Benicewicz BC, Decho AW. Nanoparticles as antibiotic-delivery vehicles (ADVs) overcome resistance by MRSA and other MDR bacterial pathogens: the grenade hypothesis. *J Glob Antimicrob Resist*. 2020;22:811–817. doi:10.1016/j.jgar.2020.06.023
20. Ionescu OM, Iacob AT, Mignon A, et al. Design, preparation and in vitro characterization of biomimetic and bioactive chitosan/polyethylene oxide based nanofibers as wound dressings. *Int J Biol Macromol*. 2021;193(Pt A):996–1008. doi:10.1016/j.ijbiomac.2021.10.166
21. Mao Z, Bai J, Jin X, Mao W, Dong Y. Construction of a multifunctional 3D nanofiber aerogel loaded with ZnO for wound healing. *Colloids Surf B Biointerfaces*. 2021;208:112070, 1-22. doi:10.1016/j.colsurfb.2021.112070
22. Tysseling-Mattiace VM, Sahni V, Niece KL, et al. Self-assembling nanofibers inhibit glial scar formation and promote axon elongation after spinal cord injury. *J Neurosci*. 2008;28(14):3814–3823. doi:10.1523/JNEUROSCI.0143-08.2008
23. Ji W, Alvarez Z, Edelbrock AN, Sato K, Stupp SI. Bioactive nanofibers induce neural transdifferentiation of human bone marrow mesenchymal stem cells. *ACS Appl Mater Interfaces*. 2018;10(48):41046–41055. doi:10.1021/acsami.8b13653
24. Liu G, Chen XI, Zhou WU, et al. Preparation of a novel composite nanofiber gel-encapsulated human placental extract through layer-by-layer self-assembly. *Exp Ther Med*. 2016;11(4):1447–1452. doi:10.3892/etm.2016.3084
25. Sahab Negah S, Oliazadeh P, Jahanbazi Jahan-Abad A, et al. Transplantation of human meningioma stem cells loaded on a self-assembling peptide nanoscaffold containing IKVAV improves traumatic brain injury in rats. *Acta Biomater*. 2019;92:132–144. doi:10.1016/j.actbio.2019.05.010
26. Sahab Negah S, Khooei A, Samini F, Gorji A. Laminin-derived Ile-Lys-Val-ala-Val: a promising bioactive peptide in neural tissue engineering in traumatic brain injury. *Cell Tissue Res*. 2018;371(2):223–236. doi:10.1007/s00441-017-2717-6
27. Vigneswari S, Chai JM, Kamarudin KH, Amirul AA, Focarete ML, Ramakrishna S. Elucidating the surface functionality of biomimetic RGD peptides immobilized on Nano-P(3HB-co-4HB) for H9c2 myoblast cell proliferation. *Front Bioeng Biotechnol*. 2020;8:567693, 1-13. doi:10.3389/fbioe.2020.567693
28. Yin H, Strunz F, Yan Z, et al. Three-dimensional self-assembling nanofiber matrix rejuvenates aged/degenerative human tendon stem/progenitor cells. *Biomaterials*. 2020;236:119802, 1-13. doi:10.1016/j.biomaterials.2020.119802
29. Mishra B, Hossain S, Mohanty S, Gupta MK, Verma D. Fast acting hemostatic agent based on self-assembled hybrid nanofibers from chitosan and casein. *Int J Biol Macromol*. 2021;185:525–534. doi:10.1016/j.ijbiomac.2021.06.116
30. Serati-Nouri H, Rasoulpoor S, Pourpirali R, et al. In vitro expansion of human adipose-derived stem cells with delayed senescence through dual stage release of curcumin from mesoporous silica nanoparticles/electrospun nanofibers. *Life Sci*. 2021;285:119947. doi:10.1016/j.lfs.2021.119947
31. Yadav C, Chhajed M, Choudhury P, et al. Bio-extract amalgamated sodium alginate-cellulose nanofibres based 3D-sponges with interpenetrating BioPU coating as potential wound care scaffolds. *Mater Sci Eng C Mater Biol Appl*. 2021;118:111348. doi:10.1016/j.msec.2020.111348
32. Cai M, Zhang G, Li C, Chen X, Cui H, Lin L. Pleurotus eryngii polysaccharide nanofiber containing pomegranate peel polyphenol/chitosan nanoparticles for control of E. coli O157: H7. *Int J Biol Macromol*. 2021;192:939–949. doi:10.1016/j.ijbiomac.2021.10.069
33. Fan H, Qiu L, Fedorov A, Willinger MG, Ding F, Huang X. Dynamic State and active structure of Ni–Co catalyst in carbon nanofiber growth revealed by in situ transmission electron microscopy. *ACS nano*. 2021;15(11):17895–17906. doi:10.1021/acsnano.1c06189
34. Saltik Cirkin D, Yuksek M. Fibroin nanofibers production by electrospinning method. *Turk J Chem*. 2021;45(4):1279–1298. doi:10.3906/kim-2011-36
35. Connolly P, Hannah AJ, Ward AC. Rapid detection of wound pathogen proteus mirabilis using disposable electrochemical sensors. 7$^{th}$World Congresso on Eletrical Engineering and Computer System Science. 2021. ICBES 105:1-8. doi:10.11159/icbes21.105
36. Song Z, Sun H, Yang Y, et al. Enhanced efficacy and anti-biofilm activity of novel nanoemulsions against skin burn wound multi-drug resistant MRSA infections. *Nanomedicine*. 2016;12(6):1543–1555. doi:10.1016/j.nano.2016.01.015
37. Sun Y, Li W, Wu X, et al. Functional self-assembling peptide nanofiber hydrogels designed for nerve degeneration. *ACS Appl Mater Interfaces*. 2016;8(3):2348–2359. doi:10.1021/acsami.5b11473
38. Shin YC, Lee JH, Kim MJ, et al. Stimulating effect of graphene oxide on myogenesis of C2C12 myoblasts on RGD peptide-decorated PLGA nanofiber matrices. *J Biol Eng*. 2015;9(1):22, 1-1. doi:10.1186/s13036-015-0020-1
39. Hsu YI, Yamaoka T. Improved exposure of bioactive peptides to the outermost surface of the polylactic acid nanofiber scaffold. *J Biomed Mater Res B Appl Biomater*. 2020;108(4):1274–1280. doi:10.1002/jbm.b.34475
40. Ong SG, Ming LC, Lee KS, Yuen KH. Influence of the encapsulation efficiency and size of liposome on the oral bioavailability of griseofulvin-loaded liposomes. *Pharmaceutics*. 2016;8(3):25, 1-17. doi:10.3390/pharmaceutics8030025
41. Schoolaert E, Cossu L, Becelaere J, et al. Nanofibers with a tunable wettability by electrospinning and physical crosslinking of poly(2-n-propyl-2-oxazoline). *Mater Des*. 2020;192:108747, 1-12. doi:10.1016/j.matdes.2020.108747
42. Shibata M, Enjoji M, Sakazume K, Ifuku S. Bio-based epoxy/chitin nanofiber composites cured with amine-type hardeners containing chitosan. *Carbohydr Polym*. 2016;144:89–97. doi:10.1016/j.carbpol.2016.02.033
43. Chen H, Cheng J, Cai X, et al. pH-switchable antimicrobial supramolecular hydrogels for synergistically eliminating biofilm and promoting wound healing. *ACS Appl Mater Interfaces*. 2022;14(16):18120–18132. doi:10.1021/acsami.2c00580
44. Wang B, Wei PW, Yao Y, et al. Functional and expression characteristics identification of Phormicins, novel AMPs from Musca domestica with anti-MRSA biofilm activity, in response to different stimuli. *Int J Biol Macromol*. 2022;209(Pt A):299–314. doi:10.1016/j.ijbiomac.2022.03.204
45. Asadi N, Mehdipour A, Ghorbani M, Mesgari-Abbasi M, Akbarzadeh A, Davaran S. A novel multifunctional bilayer scaffold based on chitosan nanofiber/alginate-gelatin methacrylate hydrogel for full-thickness wound healing. *Int J Biol Macromol*. 2021;193(Pt A):734–747. doi:10.1016/j.ijbiomac.2021.10.180